Photovoltaic Restoration of Sight with High Visual Acuity in Rats with Retinal Degeneration

D. Palanker[1,2], G. Goetz[1], H. Lorach[1], Y. Mandel[1], R. Smith[4], D. Boinagrov[1], X. Lei[3], T. Kamins[3], J. Harris[3], K. Mathieson[5], A. Sher[4]

[1]Hansen Experimental Physics Laboratory, [2]Department of Ophthalmology, [3]Department of Electrical Engineering, Stanford University, Stanford, CA 94305, USA.
[4]Institute for Particle Physics, University of California Santa Cruz, Santa Cruz, CA 95064, USA.
[5]Institute of Photonics, University of Strathclyde, Glasgow, Scotland G4 0NW, UK.

ABSTRACT

Patients with retinal degeneration lose sight due to gradual demise of photoreceptors. Electrical stimulation of the surviving retinal neurons provides an alternative route for delivery of visual information. Subretinal photovoltaic arrays with 70μm pixels were used to convert pulsed near-IR light (880-915nm) into pulsed current to stimulate the nearby inner retinal neurons. Network-mediated responses of the retinal ganglion cells (RGCs) could be modulated by pulse width (1-20ms) and peak irradiance (0.5-10 mW/mm^2). Similarly to normal vision, retinal response to prosthetic stimulation exhibited flicker fusion at high frequencies, adaptation to static images, and non-linear spatial summation. Spatial resolution was assessed in-vitro and in-vivo using alternating gratings with variable stripe width, projected with rapidly pulsed illumination (20-40Hz). In-vitro, average size of the electrical receptive fields in normal retina was 248±59μm – similar to their visible light RF size: 249±44μm. RGCs responded to grating stripes down to 67μm using photovoltaic stimulation in degenerate rat retina, and 28μm with visible light in normal retina. In-vivo, visual acuity in normally-sighted controls was 29±5μm/stripe, vs. 63±4μm/stripe in rats with subretinal photovoltaic arrays, corresponding to 20/250 acuity in human eye. With the enhanced acuity provided by eye movements and perceptual learning in human patients, visual acuity might exceed the 20/200 threshold of legal blindness. Ease of implantation and tiling of these wireless arrays to cover a large visual field, combined with their high resolution opens the door to highly functional restoration of sight.

Keywords: retinal prosthesis, retinal degeneration, restoration of sight, phovoltaic

1. INTRODUCTION

Retinal degenerative diseases such as age-related macular degeneration and retinitis pigmentosa lead to blindness due to gradual loss of photoreceptors, while the inner retinal neurons survive to a large extent(*1, 2*), albeit with sometimes extensive rewiring(*3, 4*). Retinal prostheses aim at restoring sight by electrical stimulation of these surviving neurons. In the epiretinal approach, the primary targets of stimulation are the retinal ganglion cells (RGCs) (*5, 6*), while subretinal stimulation elicits visual responses via inner retinal neurons (primarily bipolar cells) (*7-9*). Both approaches have been recently approved for clinical use, but the current clinical systems involve bulky implanted electronics with trans-scleral cables, and require very complex surgeries. In addition, visual acuity with the epiretinal system (ARGUS II, Second Sight Inc., USA) is no better than 20/1260 (*6*), and the percepts are distorted due to axonal stimulation(*10*). Subretinal prostheses (Retina Implant AG, Germany) provided similar acuity levels, except for one patient who reached 20/550 (*11*).

We developed an alternative approach to retinal prosthetics, in which photovoltaic subretinal pixels convert pulsed light into electric current, and are therefore completely wireless(*12, 13*). Bright pulsed illumination is provided by image projection from video goggles and avoids photophobic effects by using near-infrared (NIR, 880-915nm) light. Such pulsed illumination is necessary to allow capacitive discharge of the electrodes and provide charge-balanced stimulation, which is critical for safety. Optical delivery of the visual information preserves the natural link between ocular movement and image perception, unlike systems where the electrodes are connected to an external camera via

serial telemetry. Photovoltaic arrays with 3 diodes per pixel can safely elicit and modulate retinal responses, both in-vitro(*14*) and in-vivo(*15*), in normally sighted (Wild Type, WT) and in blind (Royal College of Surgeons, RCS) rats.

In this study we evaluate spatio-temporal characteristics of prosthetic vision, including one of its most important properties: the spatial resolution of the retinal response in-vitro and visual acuity in-vivo.

2. RESULTS AND DISCUSSION

2.1 Photovoltaic arrays

The prosthetic devices used throughout the study consisted of a hexagonal array of 70µm pixels separated by 5µm trenches(*13*) (Fig. 1). Pixels consisted of several photodiodes connected in series, delivering anodic-first charge-balanced current pulses. The fabrication process was similar to the one described by Wang et al. (*16*) for cathodic polarity, with the n-doped and p-doped regions reversed, in order to produce anodic-first pulses. In these pixels, 2 or 3 diodes are connected in series between the active disc electrode 20 µm in diameter and a circumferential ring return electrode of 5 µm in width (Fig. 1), producing well-confined electric fields, with low cross-talk between neighboring pixels.

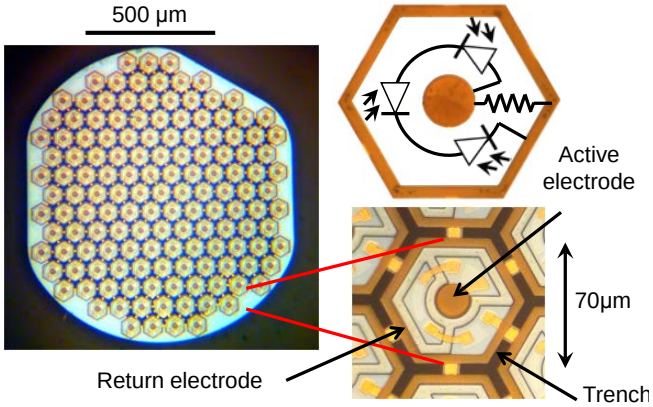

Figure 1. The prosthesis is composed of 70µm pixels separated by 5µm trenches arranged in a 1mm-wide hexagonal pattern. Each pixel consists of two to three (shown here) photodiodes connected in series between the central active and surrounding return electrode.

2.2 Electrical receptive fields

In-vitro evaluation of the spatial resolution of the retinal response to photovoltaic stimulation and to visible light was conducted by recording from hundreds of retinal ganglion cells (RGCs) in the rat retina using a large-scale multi-electrode array system. We mapped the electrical receptive fields (eRFs) of the RGCs using a sparse NIR binary noise stimulus projected onto the photovoltaic pixels. The average eRF diameter was 248±59µm in WT and 203±63µm in degenerate RCS retinas. With visible light, the average diameter of the WT vRFs was 249±44µm, not significantly different from the measured eRF sizes.

2.3 Retinal response to grating contrast reversal

While measuring spatial extent of electrical receptive fields obtained with a sparse white noise provides an estimate of achievable spatial resolution, it does not take into account possible non-linear effects of presenting more complex stimuli. In order to account for this, we characterized retinal responses to alternating square gratings of various spatial frequencies using visible light and photovoltaic stimulation. This type of stimulus is routinely used for measuring visual acuity in-vivo(*17*).

In the majority of the ganglion cells in RCS retinas, electrical stimulation at 20Hz resulted in flicker fusion. With both, electrical (RCS) and visible light (WT) stimulation, the majority of RGCs only responded to the contrast reversal of the gratings and not to every pulse of light, illustrating this flicker fusion and adaptation to static images. The RGC response to grating contrast reversal as a function of the stripe width decreased with increasing spatial frequency of the gratings, both with visible light and electrical stimulation. Stimulation thresholds were defined as a 50% probability of eliciting an action potential correlated with the grating contrast reversal. With visible light the number of responding cells peaked at a stripe width of 28µm. With photovoltaic stimulation, the narrowest resolvable stripes were 67µm.

Responses of the neurons to gratings smaller than their receptive field diameter, whether electrical or visible, can be explained by non-linear interactions in receptive field subunits (*18-20*). For visible light, the peak corresponds to neurons responding to each phase of the grating alternation. This classical frequency doubling of the response is indicative of nonlinear spatial summation (*18, 20*). Similarly, neurons responded in NIR to gratings with 67µm stripe width in each phase of the grating alternation, i.e. with frequency doubling. This demonstrates non-linear summation inside the RGC electrical receptive fields, with the size of the effective non-linear subunits comparable to our pixel pitch (65µm). All neurons that exhibited complete flicker fusion with photovoltaic stimulation (i.e., no response to 20 Hz

pulses without the change of the projected image) responded to alternation of gratings with stripe widths smaller than 100µm.

2.4 Sub-retinal implantations in-vivo

For in-vivo testing of prosthetic vision we implanted the photovoltaic arrays subretinally in wild-type rats and in rats with retinal degeneration. All experimental procedures were conducted in accordance with the institutional guidelines and conformed to the Statement for the Use of Animals in Ophthalmic and Vision research of the Association for Research in Vision and Ophthalmology (ARVO) and in accordance with the Code of Ethics of the World Medical Association (Declaration of Helsinki). All animals were housed in an environment with a 12-h light/12-h dark cycle with food and water ad libitum. Rats with retinal degeneration were obtained from a Royal College of Surgeons (RCS) colony maintained at the Stanford Animal facility.

For surgeries, animals were anesthetized with Ketamine (75mg/kg) and Xylazine (5mg/kg) delivered by intramuscular injection. Subretinal implantations were performed as previously described [8]. Briefly, the sclera and choroid were incised to create a retinal detachment using saline solution, and the implant was inserted into the subretinal space. The incision was then sutured and treated with a local antibiotic (Bacitracin/Polymyxin B). In animals implanted with active devices (15WT and 7RCS) cortical screw electrodes were implanted over the visual cortex on both hemispheres 4mm lateral from midline, 6mm caudal to the bregma, as previously described [8] to measure visually evoked potentials (VEP).

To control the success of the subretinal implantation and assess the health of the retina above the implant, we conducted optical coherence tomography (OCT) and fluorescence angiography (FA) one week after implantation (HRA2-Spectralis, Heidelberg Engineering, Heidelberg, Germany). Fluorescein angiography confirmed normal retinal blood perfusion above the implant. Optical coherence tomography (OCT) performed one week after surgery demonstrated close and stable proximity of the inner nuclear layer to the implant (Figure 2). In WT rats, the presence of the subretinal implant caused degeneration of photoreceptors above the chip, while the inner nuclear layer (INL) and ganglion cell layer (GCL) were well preserved.

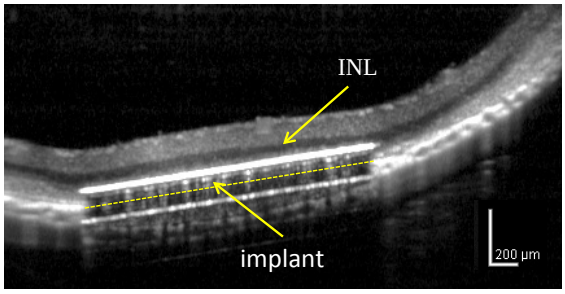

Figure 2. OCT shows good preservation of the inner retina, with the inner nuclear layer (INL) located approximately 20µm above the upper surface of the implant. Thickness of the implant appears larger than 30µm due to its high refractive index. The yellow dash line illustrates the actual position of the implant's back side on top of RPE.

2.5 Visual acuity

Response of the visual system was assessed by recording visually evoked potentials (VEPs) induced either by the implant activated with pulsed NIR light (eVEP), or by visible light projected onto normal retina. One of the established methods for assessing visual acuity in animals and in human infants is based on cortical response to alternating gratings of various spatial frequencies, recorded through visually evoked potentials (VEPs)(*17*).

We recorded the cortical responses to such alternating NIR patterns in implanted RCS rats and to the same patterns presented with visible light in WT animals outside of the implanted area where the retina is preserved. The square-wave grating patterns were projected using 4ms pulses at 40Hz repetition rate, reversing the contrast at 2Hz. Grating stripe width varied from 6µm to 200µm. The VEP amplitude decreased with increasing spatial frequency for both visible and electrical stimulation (Figure 3). The

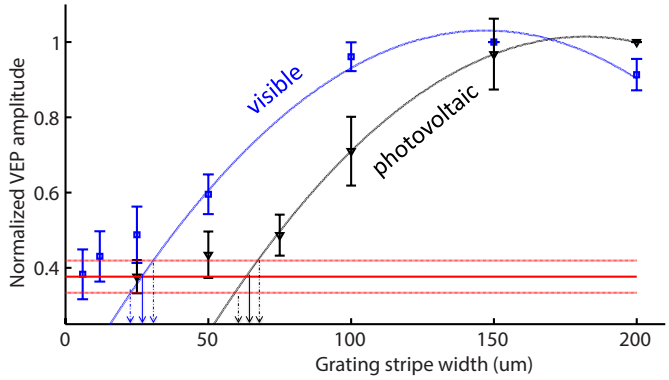

Figure 3. VEP amplitude for alternating gratings projected by visible light (blue) and prosthetic stimulation (black) decrease with decreasing width of the stripes. Acuity limit, estimated as the crossing point of the parabolic fits with the noise level (red lines), corresponds to 29±5µm/stripe for visible light and 63±4µm/stripe for prosthetic stimulation.

acuity limit was estimated by extrapolating the measured data down to the noise level. For prosthetic vision in RCS rats, it yielded 63±4μm per stripe, as compared to 29±5μm per stripe in WT animals stimulated with visible light. These results correspond to 0.48 and 1 cycle per degree (cpd) respectively, in close agreement with the visual acuity of pigmented rats reported in the literature(*17, 21*).

To confirm that these responses were conveying spatial information rather than charge accumulation or an illumination misbalance between the two phases of the grating, we recorded the stimuli on the cornea and reproduced similar transitions with a full-field stimulus devoid of spatial content. For all grating sizes, the equivalent spatially uniform stimulus did not trigger any significant VEP response, thus confirming that the grating response did involve spatial modulation. Additionally, RCS rats did not respond to alternating gratings projected onto the implanted area with visible light, and did not respond to pulsed infrared light projected away from the implant either.

3. CONCLUSIONS

If the spatial localization from our measurements will translate to the human retina, such prosthetic performance would correspond to visual acuity of 20/250, which is well below the legal blindness limit of 20/400, as defined by the World Health Organization. With the enhanced acuity provided by eye movements and perceptual learning in patients, visual acuity could perhaps cross the 20/200 threshold of legal blindness in the US.

Stimulation thresholds of 0.33mW/mm^2 with 10ms pulses, observed in these studies are more than two orders of magnitude below the ocular safety limits for NIR radiation(*22*). Such a wide range of safe stimulation may allow futher reduction of the pixel size, up to a factor of 2. Ease of implantation and tiling of these wireless arrays to cover a large visual field, combined with their high resolution opens the door to highly functional restoration of sight.

REFERENCES

1. A. Santos et al., Preservation of the inner retina in retinitis pigmentosa: A morphometric analysis. Archives of Ophthalmology 115, 511 (1997).
2. M. S. Humayun et al., Morphometric analysis of the extramacular retina from postmortem eyes with retinitis pigmentosa. Invest Ophthalmol Vis Sci 40, 143 (1999).
3. R. E. Marc, B. W. Jones, C. B. Watt, E. Strettoi, Neural remodeling in retinal degeneration. Progress in Retinal and Eye Research 22, 607 (2003).
4. B. W. Jones, R. E. Marc, Retinal remodeling during retinal degeneration. Experimental eye research 81, 123 (2005).
5. M. R. Behrend, A. K. Ahuja, M. S. Humayun, R. H. Chow, J. D. Weiland, Resolution of the Epiretinal Prosthesis is not Limited by Electrode Size. IEEE Transactions On Neural Systems And Rehabilitation Engineering 19, 436 (2011).
6. M. S. Humayun et al., Interim results from the international trial of Second Sight's visual prosthesis. Ophthalmol. 119, 779 (2012).
7. E. Zrenner, Fighting Blindness with Microelectronics. Science Translational Medicine 5, 210 (2013).
8. R. J. Jensen, J. F. Rizzo, 3rd, Thresholds for activation of rabbit retinal ganglion cells with a subretinal electrode. Exp Eye Res 83, 367 (Aug, 2006).
9. E. Zrenner et al., Subretinal electronic chips allow blind patients to read letters and combine them to words. Proceedings of the Royal Society B: Biological Sciences, (2010).
10. D. Nanduri et al., Frequency and Amplitude Modulation Have Different Effects on the Percepts Elicited by Retinal Stimulation. Investigative Ophthalmology & Visual Science 53, 205 (2012).
11. K. Stingl et al., Artificial vision with wirelessly powered subretinal electronic implant alpha-IMS. Proc Biol Sci 280, 20130077 (2013).
12. K. Mathieson et al., Photovoltaic Retinal Prosthesis with High Pixel Density. Nat Photonics 6, 391 (Jun 1, 2012).
13. L. Wang et al., Photovoltaic retinal prosthesis: implant fabrication and performance. J Neural Eng 9, 046014 (2012).
14. K. Mathieson et al., Photovoltaic retinal prosthesis with high pixel density. Nature Photonics 6, 391 (2012).
15. Y. Mandel et al., Cortical responses elicited by photovoltaic subretinal prostheses exhibit similarities to visually evoked potentials. Nature communications 4, 1980 (2013).

16. L. Wang et al., Photovoltaic retinal prosthesis: implant fabrication and performance. Journal of Neural Engineering 9, 046014 (2012).
17. L. C. L. Silveira, C. A. Heywood, A. Cowey, Contrast Sensitivity and Visual-Acuity of the Pigmented Rat Determined Electrophysiologically. Vision Res 27, 1719 (1987).
18. W. F. Heine, C. L. Passaglia, Spatial receptive field properties of rat retinal ganglion cells. Visual Neuroscience 28, 403 (2011).
19. C. Enroth-Cugell, J. G. Robson, The Contrast Sensitivity of Retinal Ganglion Cells of the Cat. J. Physiol. 187, 517 (1966).
20. D. Petrusca et al., Identification and characterization of a Y-like primate retinal ganglion cell type. The Journal of neuroscience : the official journal of the Society for Neuroscience 27, 11019 (Oct 10, 2007).
21. G. T. Prusky, P. W. West, R. M. Douglas, Behavioral assessment of visual acuity in mice and rats. Vision Res 40, 2201 (2000).
22. J. D. Loudin, S. F. Cogan, K. Mathieson, A. Sher, D. V. Palanker, Photodiode Circuits for Retinal Prostheses. IEEE Transactions on Biomedical Circuits and Systems, 5, 468 (Oct. 2011).